Differential Scanning Calorimetry Study of the Structure of Water Confined within AOT Lamellar Mesophases

Eric Prouzet,*,† Jean-Blaise Brubach,‡ and Pascale Roy*,‡

Chemistry & Waterloo Institute of Nanotechnology, University of Waterloo, 200 University Av. West, Waterloo, Ontario N2L 3G1, Canada, and SOLEIL, CNRS, L'Orme des Merisiers, St-Aubin BP48, 91192 Gif-sur-Yvette Cedex, France

Received: February 6, 2010; Revised Manuscript Received: April 23, 2010

We combined thermal analysis with FT-IR measurements to solve the structure of the water network confined within lamellar bilayers of AOT surfactant. Unlike previous FT-IR analyses that allowed us only to point out spectroscopic molecular components characterized by their local connectivity, differential scanning calorimetry (DSC) allowed us to identify homogeneous thermal populations listed as low, medium and high temperature. HT water was identified with bulk water, and LT water, as hydration water closely linked with surfactants heads. MT water was assigned to a disrupted network of water corresponding to a layer of 0.5 nm modified by the effect of confinement created by the vicinity of the surfactant bilayer. It appears from this study that the actual extent of confinement influence is lower than expected, at least for lamellar structures. Each thermal population was finally described by a different distribution of the spectroscopic components identified in parallel by FT-IR.

Introduction

The structural modifications of water submitted to confinement effects or surface interactions, are of great interest in several areas, such as materials science, biology, or geology, all disciplines that deal with multicomponent systems.[1] Indeed, water is a highly correlated system, where molecules withstand dynamic interactions through hydrogen bonds. Formation of large clusters and long-range water networks result from these interactions.[2−5] The interest for studying this system as well as the influence of external parameters such as confinement, has been growing, and numerous studies have demonstrated that the intermolecular structure of water is modified by various interactions including salt surfactants, biologic components, surfaces, and liquid crystals[6−11] or under confining conditions such as in reverse microemulsions, solid matrix, glycolipid nanotubes, or droplets and thin films.[3,4,12−19]

FT-IR has been widely used for the determination of the different types of water population by the analysis of the OH stretching bond in the 3300−3700 cm^{-1} region of the IR spectrum.[12] It was frequently applied onto the AOT-based (bis(2-ethylhexyl)sulfosuccinate sodium salt) phases, either in W/O reverse microemulsions or in lamellar liquid crystals because the latter allow a wide range of dimensions (either spherical or lamellar) for the water phase, from highly confined systems to almost "free" water. However, direct assignment of the IR contributions to actual types of water populations is not straightforward because this technique provides only information on the local state, that is, the different types of water molecules identified by their connectivity with others. There have been generally three spectroscopic components identified and these components are observed in bulk water, which demonstrates that the spectroscopic components identified by IR cannot be assigned to an actual type of water, taken as a whole, but to the molecular species present within. Due to this uncertainty, the water structure in reverse microemulsions was described with different views. Onori described it as a mixture of "*bonded*" and "*bulk*" water.[13] On the contrary, Novaki et al. came to the conclusion that the "*aggregate-solubilized*" water had a structure different from bulk water, but that it could not be described as made of layers of different structures.[4] A first assignment of the three components present even in bulk water, in terms of hydrogen-bonding, was made by Temsamani et al. with components of the OH-stretching peak related with linear and fully developed H-bonds, distorted structures, and free hydroxyl groups.[15] Brubach et al. were first to associate these components with the connectivity of water molecules. They sorted the different types of molecules with the number of H-bonds they were involved in, leading to highly connected "*network*" molecules (3295 cm^{-1}), "*intermediate*" water molecules (3460 cm^{-1}), and loosely connected "*multimer*" water molecules (3640 cm^{-1}).[16,17,19] On the other side, simulations based on dissipative particle dynamics (DPD) identified three populations as bulky water, bound water around surfactant heads, and trapped water close to the hydrophobic palisade.[18]

These studies were extended to lamellar liquid crystals made with water/AOT mixtures. Lamellar phases constitute a complementary model that helps to increase the understanding of water confining in a larger domain of water thickness from highly confined structures to almost bulk-like water.[6,9] The analysis of the OH stretching peak was made according to the Brubach's components model.[16]

All these studies led roughly to the same description of the water molecular species defined according to their H-bond connectivity. However, the question still arose to how the structure of confined water can be described and if it would be possible to decide between two models that are either the existence of three different populations of water giving three different FT-IR contributions as stated by example by Yuan[18]

* Corresponding authors. E-mail: E.P., eprouzet@scimail.uwaterloo.ca; P.R., pascale.roy@synchrotron-soleil.fr.
† University of Waterloo.
‡ CNRS.

10.1021/jp101176v
Published on Web 05/28/2010

TABLE 1: Analysis of the DSC Peaks of Melting of Water

				DSC Peak 1 (LT)			DSC Peak 2 (MT)			DSC Peak 3 (HT)		
AOT (wt%)	t (nm)[d]	raw melting enthalpy (J/g)[a]	water melting Enthalpy (J/g)[b]	T (°C)[c]	LT enthalpy (J/g)	LT enthalpy (%)	T (°C)[c]	MT enthalpy (J/g)	MT enthalpy (%)	T (°C)[c]	HT enthalpy (J/g)	HT enthalpy (%)
7.5[e]		296.6	320	–11.4	0.6	**0.2**	–9.7	1.0	**0.3**	–2.2	318.4	**99.5**
10	18.6	295	328	–11.8	1.3	**0.4**	–9.4	1.6	**0.5**	–2.7	325.0	**99.1**
15	13.25	243.7	325	–11.7	1.3	**0.4**	–10.1	4.2	**1.3**	–2.3	319.0	**98.2**
25	7.77	236.5	315	–12.5	3.8	**1.2**	–10.0	11.3	**3.6**	–3.0	299.9	**95.2**
30	5.56	212	303	–12.2	3.9	**1.3**	–10.5	19.7	**6.5**	–3.0	279.4	**92.2**
40	3.45	163.2	272	–12.2	3.0	**1.1**	–11.2	32.1	**11.8**	–2.7	236.9	**87.1**
50	2.4	126.7	253	–11.9	4.5	**1.8**	–11.6	63.2	**25.0**	–3.3	185.2	**73.2**
54	2.06	111.9	243	–11.7	4.4	**1.8**	–11.1	67.5	**27.8**	–3.2	171.1	**70.4**
60	1.5	89.4	223	–11.8	10.7	**4.8**	–10.4	84.7	**38.0**	–3.5	127.1	**57.0**
70		45	150	–11.6	12.0	**8.0**	–11.1	131.0	**87.3**	–3.1	7.0	**4.7**
80		1.97	9.85	–11.3	3.1	**31.8**	–10.7	6.7	**68.2**		0.0	**0.0**

[a] Measured on the DSC curve. [b] Normalized to the water amount. [c] Taken at the onset point. [d] Water thickness $t = d_{001} - 1.9$. [e] No lamellar phase.

or that of a continuum of configurations schematically divided in three parts, as proposed by Novaki.[4]

In parallel, differential scanning calorimetry (DSC) provides information on uniform thermal populations, not individual entities, but it cannot describe precisely their structure.[5,7,10,11,20,21] When comparing with FT-IR, one may assume that a single peak observed in DSC is the fingerprint of an energetically homogeneous population.[21] This means that DSC provides information about the different water networks whereas IR lists the different molecules (sorted by their degree of H-bond connection) within these networks. Therefore, combination of IR and DSC is highly suitable for the study of systems that are temperature dependent. Inoue et al. studied the phase diagram of $C_{12}E_7/H_2O$ by DSC and FT-IR and pointed out the occurrence of three types of endothermic peaks between −10 and 0 °C, which were assigned to phase transitions: solid → H1 (normal hexagonal) → V1 (normal bicontinuous-type cubic) → LR (lamellar) → liquid.[7] Lamellar AOT phases analyzed by DSC clearly revealed three endothermic peaks that were analyzed differently depending on the authors, either as the signal of two types of water plus surfactant melting[20] or as three types of water.[21] Finally, Ciesla et al., in a study on interaction of water with a cellulose membrane, pointed out that one to three endothermic peaks could be identified and related with melting of bulk and interfacial water, during the heating cycle.[10] It was, from our knowledge, the first time that a parallel assignment like those deduced from FT-IR, was made from DSC measurements on confined water.

We report in this study the results of DSC analysis on lamellar phases of AOT studied in a broad range of concentration. These results, compared with previous and new FT-IR experiments, allowed us to propose a model for the water structure confined within the AOT bilayers.

Experimental Section

AOT (bis(2-ethylhexyl)sulfosuccinate sodium salt) from Fluka (98% grade) was used as received. Samples were prepared from a 5−80 AOT/H_2O wt % composition range (Table 1). Samples were kept in sealed flasks for at least 2 months to let them become homogeneous. The water thickness of the different lamellar samples was determined by small angle X-ray diffraction (SAXD). The diffraction patterns of mesophases with different concentrations, were recorded with an in-house diffractometer equipped with a copper rotating anode X-ray source (4 kW) and a multilayer focusing "OSMIC" monochromator giving the Cu−Kα radiation (wavelength $\lambda = 0.154$ nm), a high flux (10^8 photons/s), and a punctual collimation. The diffraction pattern was collected with a two-dimensional image plate detector and further transformed in the radial scattering pattern. Samples were sealed in 1.5 mm thick glass Lindeman capillaries, and measurements were carried out in a transmission configuration with recording time of 30 min. Due to the sample high intensity scattering level, the X-ray diffraction patterns were not corrected for any background scattering.

FT-IR spectra for samples at room temperature were obtained after 32 scans with a Nicolet Nexus FT-IR equipped with an Imaging Golden Gate Diamond ATR head. Description of the OH stretching 3000 cm^{-1} FT-IR region was given in previous reports.[9,16,17] Peak analysis was performed according to previous assignments made for the OH stretching band of water molecules: "network" water (NW) (≈3300 cm^{-1}), "intermediate" water (IW) (≈3450 cm^{-1}), and "multimer water" (MW) (≈3550 cm^{-1}). Peak fitting proceeded through a three-Gaussian fit, each function corresponding to one of the previous spectroscopic populations as identified by Brubach et al.[17] The 1600 cm^{-1} region contains bands of OH bending (≈1650 cm^{-1}) and CO stretching bands (≈1720 and 1736 cm^{-1}) arising from two nonequivalent groups in the AOT molecules.[6] This domain was fitted with two Gaussian functions because the CO bands could not being discriminated.

DSC measurements were performed on a 2920 TA-Instrument Modulated MDSC with two complete thermal cycles between +25 and −35 °C, with a 5 °C min^{-1} ramp. The first down and up cycle was used only to apply the same thermal history to all samples. Only the second increasing ramp was analyzed. The comparison between the two rising ramps allowed us to check that no water evaporation had occurred during the analysis. As DSC peaks are merged, we fitted them with Gaussian functions, which are not the expected shape but allowed us to decrease the amount of fitting parameters. The melting temperature for each contribution was determined at the onset point tangent to the left side of the peak. All signals were normalized with the amount of water.

Results

An example of the DSC signal upon thermal cycling is displayed in Figure 1. Every single peak in the DSC signal is the signature of a thermally homogeneous population that exhibits a first order phase transition. The heating ramp exhibits three well-defined endothermic peaks that are repeated from cycle to cycle and present in different proportions for all AOT concentrations.[20,21]

The evolution of these melting peaks with the AOT concentration is plotted in Figure 2, for compositions ranging between

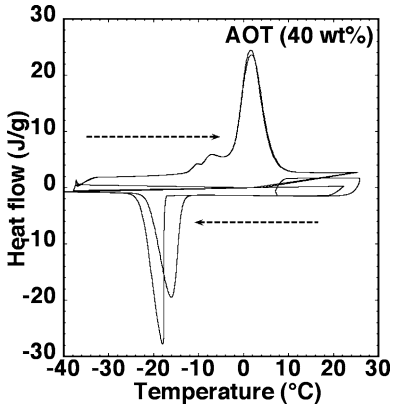

Figure 1. Example of a raw DSC spectrum recorded for the 40 wt % AOT sample. This curve was recorded with two successive cycles, starting from +25 °C down to −35 °C and up. The second heating ramp was used for analysis.

15 and 60 wt % AOT (dashed curves) (the 80 wt % sample is plotted with black dots). From the peaks onset points, we identified a "low" temperature peak (LT) at about −12 °C, a "medium" one (MT) around −10 °C, and a "high" one (HT) close to −2 °C. This result demonstrates that water confined in AOT bilayers is composed of three specific thermal populations. As the AOT concentration increases, one observes a decrease in intensity of the HT peak in parallel with the rising intensity of the MT peak (Figure 2).

Fitting results are reported in Table 1 (for examples of peak fitting, see Figure SI.1 in the Supporting Information). A linear relationship between the d_{001} spacing of the lamellar phase determined by SAXD and the water thickness t between two double layers of surfactant has been established previously according to[9]

$$t\,(\mathrm{nm}) = d_{001} - 1.9 \qquad (1)$$

t can be ascribed only for AOT compositions ranging between 10 and 60 wt %, within the lamellar structure range. Below it, vesicles are observed, and above it, the lamellar composition transforms into a cubic structure. The evolution of the melting temperature for each population as a function of t is reported in Figure 3. As t decreases from 19 to 2 nm, the LT melting temperature decreases slightly from −11.7 to −12.4 °C, as well as the temperature of HT population, which stands only a slight decrease from −2.5 to −2.9 °C, both within the error range. MT water displays a steady evolution of the melting temperature with t from −9.4 to −11 °C, which appears to be more significant.

The total enthalpy of melting was evaluated for the temperature range between −15 and +15° (Table 1) with the DSC peaks normalized to the water amount for each sample once we had checked that the surfactant alone does not contribute to any thermal event in this region. As observed in the inset of Figure 4, the total enthalpy decreases with the water thickness, which implies that populations with a lower enthalpy of melting become predominant. The respective proportions of each thermal contribution as a function of t are reported in Figure 4. From t = 7 nm down to 1 nm, the proportion of the HT enthalpy to the total signal drops down whereas that of the MT peak (peak 2) increases. The LT peak (pPeak 1) remains rather constant. For $t \geq 7$ nm, the HT peak (peak 3) contributes to 98% of the total enthalpy, the other contributions being negligible with an enthalpy equal to 320 J g^{-1} (Table 1). This value is in good agreement with the value of 333 J g^{-1} determined by calorimetry for pure water.[22] This allows us to assign the HT peak to "bulk" water.

We checked in parallel the influence of sodium ions (counterions of AOT) on the connectivity of the water network. FT-IR study of the NaCl solutions with concentrations ranging from 0 to 2 mol L^{-1} revealed that the salt concentration has almost no effect on the three components of the OH stretching mode, which are only slightly modified with a small shift toward higher wavenumbers (Figure SI.2, Supporting Information).

These analyses were carried out in parallel with SAXD and FT-IR, as already reported.[9] SAXD patterns are displayed in Figure SI.3 and Table SI.I (Supporting Information). The evolution of the FT-IR spectra with t is similar to those previously reported (Figure 5 and Tables SI.I and SI.II, Supporting Information).[9] The OH stretching band exhibits three components, each corresponding to spectroscopic signatures of single water molecules more or less connected by hydrogen bonds and identified as NW, IW, and MW populations. As the AOT composition increases (t decreases), this band shifts toward higher wavenumbers (Figure 5a). In terms of intensity, all components remain constant above $t \approx 4$ nm (AOT wt % ≤ 50%). Below $t = 4$ nm, the MW component remains constant, and close to 12%, whereas a change is observed for both the NW and IW components, with an increasing of IW (from 13% to 23%) at the expense of NW (from 74% to 63%).

The 1600 cm^{-1} region contains also information on both the HOH bending (≈1650 cm^{-1}) and CO stretching bands (≈1720 and 1736 cm^{-1}) arising from two nonequivalent groups in the AOT molecules.[6] This region can inform about the degree of disturbance of the AOT molecules. It was fitted with only two Gaussian functions because the two CO bands could not be discriminated. The analysis reveals only a slight evolution of these bands as a function of the AOT concentration (Figure SI.4, Supporting Information) with a small shift of the HOH bending band from 1640.5 to 1644.5 cm^{-1} as t decreases from 20 to 1 nm, which could be linked with changes in hydrogen bonding, as previously assumed.[23] As for the CO stretching band, it remains constant and close to 1728.5 cm^{-1}, the slight shift toward lower wavenumber possibly arising only from mathematical fitting artifact. This result demonstrates that the internal structure of the surfactant remains unchanged whatever the AOT/water ratio.

Discussion

Structure of Water Confined within the AOT Bilayers. Among different models that have been proposed until now, the model based on IR spectroscopy identifies three spectroscopic components, named "network water" (NW) (≈3300 cm^{-1}), "intermediate water" (IW) (≈3450 cm^{-1}), and "multimer water" (MW) (≈3550 cm^{-1}), each corresponding to molecules exhibiting a given degree of connectivity, even though these molecules can belong to different thermal populations of water related to their location relative to the surfactant layer (Figure 5).[9,16,17,19] Hence, this analysis alone cannot help us to discriminate between a single population that could exhibit a continuous evolution in the connectivity from water molecules close to the surfactant up to bulk water, and the existence of several populations clearly identified. This problem is well illustrated by the IR spectrum of bulk water, a homogeneous system that displays nevertheless the three spectroscopic components.

DSC allowed us to solve this ambiguity because the observation of the melting curves points out clearly three endothermic peaks that we ascribe to three different types of water (LT, MT,

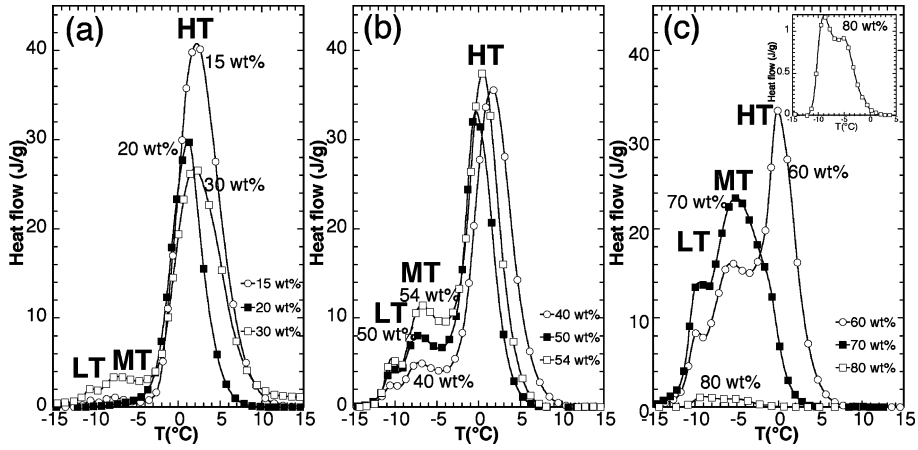

Figure 2. Evolution of the endothermic peak (normalized to the water amount) corresponding to the melting of ice, as a function of the AOT amount. We identified three peaks named as high (HT), medium (MT), and low (LT) temperatures peaks: (a) 15, 20, and 30 AOT wt %; (b) 40, 50, and 54 AOT wt %; (c) 60, 70, and 80 AOT wt % (inset in (c): magnification of the 80 wt % DSC peaks).

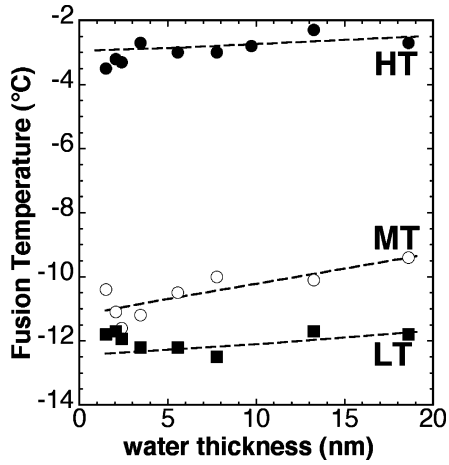

Figure 3. Temperatures of the DSC peaks for the AOT samples, taken at the onset point (left side), as a function of the water thickness t in the lamellar phases.

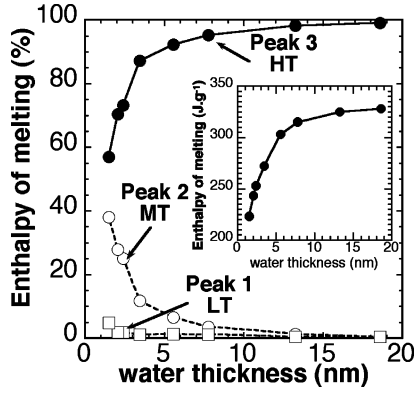

Figure 4. Evolution of the respective contributions for the three different types of thermal populations, as a function of the water thickness t between two bilayers in the lamellar phase. Inset: evolution of the total enthalpy of melting as a function of t.

HT), each being possibly made of varying proportions of molecules with different degrees of connectivity (NW, IW, MW). The DSC peak that we ascribe to the LT water had been assigned previously to surfactant freezing (melting) on the basis of NMR analysis.[20] We do not sustain this interpretation because the surfactant alone does not stand any phase transition at this temperature. Nevertheless, the melting of water molecules closely linked to the surfactant head can induce changes in the surfactant molecules, which can be probed by NMR or diffraction. This explains why this phenomenon probed by DSC, even though assigned to water melting, can lead to parallel changes in the surfactants structure. The existence of three populations (LT, MT, HT) is confirmed by their melting temperature that remains almost constant for all concentrations (Figure 3).

Therefore, on the basis of the DSC analysis, we describe the structure of water confined in AOT lamellar mesophases as made of three discrete water populations characterized by three different melting temperatures. A plot of the proposed structure is given in Scheme 1.

LT water (thickness x) is expected to be in close interaction with the surfactants heads, HT (thickness z) corresponds to nondisturbed (bulk) water localized in the central region, and MT (thickness y) is settled in the vicinity of the AOT bilayers and disturbed by it, with

$$(x_i + y_i + z_i)/t = 1 \quad (2)$$

The of water melting can be written as

$$\Delta H = \Delta H(\mathrm{LT}) + \Delta H(\mathrm{MT}) + \Delta H(\mathrm{LT}) = x\Delta H^\circ_{\mathrm{LT}} + y\Delta H^\circ_{\mathrm{MT}} + z\Delta H^\circ_{\mathrm{HT}} \quad (3)$$

ΔH° is the standard enthalpy of melting for a given population. The LT component (ΔH(LT)) is very small (<5 J g^{-1}) and rather constant up to a AOT concentration of 70 wt % thickness (Table 1 and Table 2). It must correspond at least to the molecules of hydration, which were found equal to be 2.6 per surfactant head.[9] This hydration water must be intercalated between the surfactant heads, and it will not contribute significantly to the total water thickness t.

To reduce the number of independent parameters in this analysis, we assumed in a first approximation that both the LT and MT thermal contributions could be merged and a single enthalpy of melting could be assigned to both of them. This assumption does not preclude any difference in the actual enthalpies of melting but it is justified by (i) the minor contribution of LT population, and (ii) their close temperatures of melting (≈ -11 °C) (Figure 3). Such an assumption allows us to simplify eq 3 so that eq 3 can be written as follows:

$$\Delta H \approx (x + y)\Delta H^{\circ}_{MT} + z\Delta H^{\circ}_{HT} = Y\Delta H^{\circ}_{MT} + z\Delta H^{\circ}_{HT} \quad (4)$$

Proportions between x and y are deduced from their proportions in the DSC peaks (Table 2). We calculated first the proportion z of HT water from

$$\Delta H(\mathrm{HT}) = z\Delta H^{\circ}_{HT} \quad (5)$$

ΔH°_{HT} being the melting enthalpy of bulk water (330 J g^{-1}), values of z can be easily calculated from (5) and Y values deduced simply from ($Y \approx 1 - z$) (Table 2). The knowledge of both the MT and HT populations allowed us to find the expected standard enthalpy of melting for the (LT + MT) water population according to $\Delta H^{\circ}_{MT} = \Delta H_{LT+MT}/Y$ (Table 2). For lowest values of Y (high t), the error is too large to provide an accurate estimation. On the other side, for highest values of Y (small t), the respective contribution of LT water cannot be discarded and values of ΔH°_{MT} are also questionable. In the expectation of further calorimetry measurements, we can estimate, however, that the standard enthalpy of melting for the MT water, deduced from the median samples, is close to 150 J g^{-1}. The evolution of the different populations is plotted in Figure 6 along with the parallel evolutions of water thicknesses for HT and MT water (a scheme of these structures is displayed in Scheme SI.1, Supporting Information).

MT water appears as a layer of disturbed water in the vicinity of the AOT bilayer. Its thickness increases slightly to 0.5 nm as the total thickness decreases (see Scheme SI.1, Supporting Information). The melting energy of this structure requires half that of bulk water (≈150 J g^{-1} versus 330 J g^{-1}) in line with

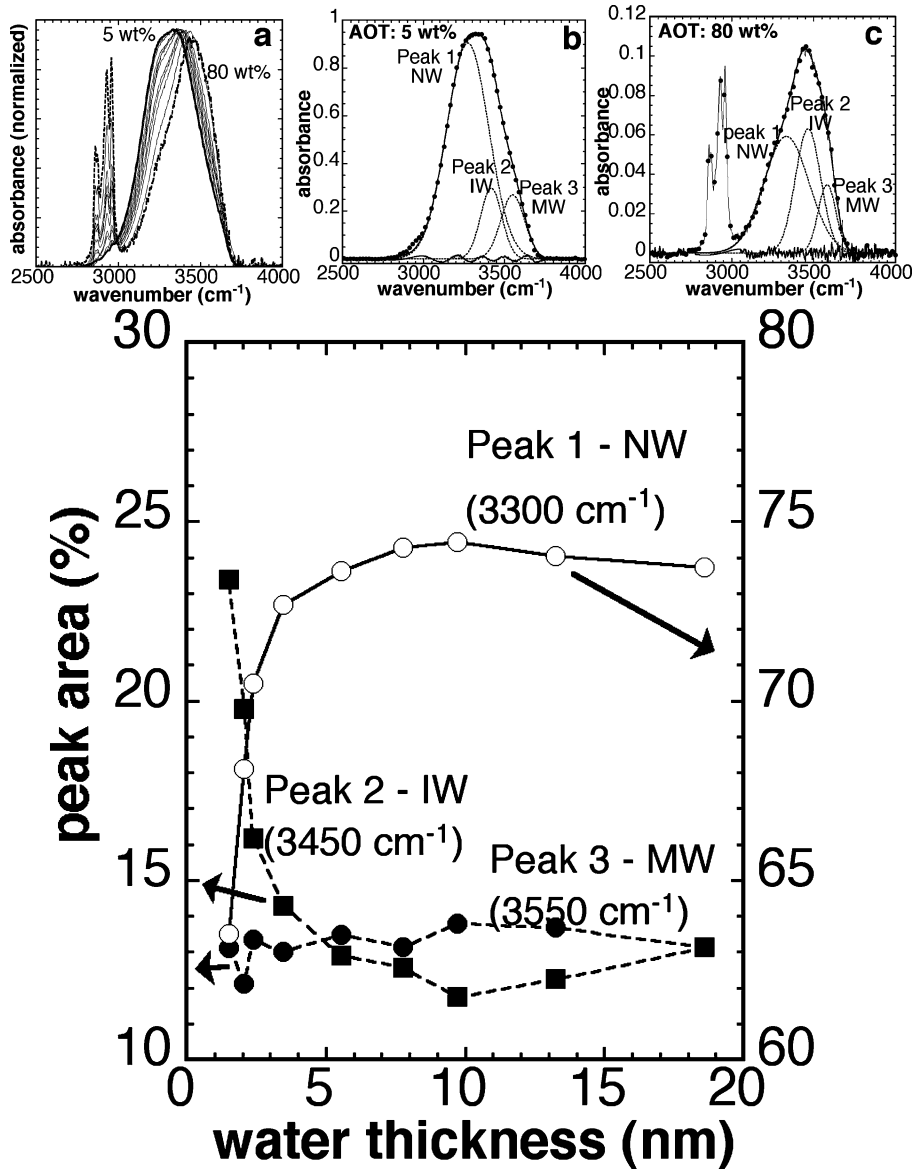

Figure 5. Top: evolution of the FT-IR peak of the OH stretching mode as a function of the AOT amount (a) and examples of fit for (b) the 5 wt % and (c) the 80 wt % AOT samples. The total surface of the peaks was normalized to ease comparison. The narrow peaks at 3000 cm^{-1} correspond to $-CH_2-$ vibration modes of the surfactant. The broad peak between 3000 and 3700 cm^{-1} corresponds to the $-OH$ stretching mode. As the AOT concentration increases from 5 to 80 wt %, the lower wavenumber part decreases and an additional shoulder at higher wavenumber appears. The OH stretching peak exhibits a major contribution of network water, even if the IW and MW contributions are also present. For higher concentrations (c), the NW part decreases and one observes an increase of the intermediate water population. Dots: experimental curve. Line: fit and residue. Dashed: single peaks. Bottom: evolution of the IR peaks areas assigned to network (NW), intermediate (IW), and multimer (MW) water spectroscopic contributions as a function of the water thickness between two bilayers in the lamellar phase.

SCHEME 1: Hypothetical Structure of the Water Volume between Two Bilayers of AOT

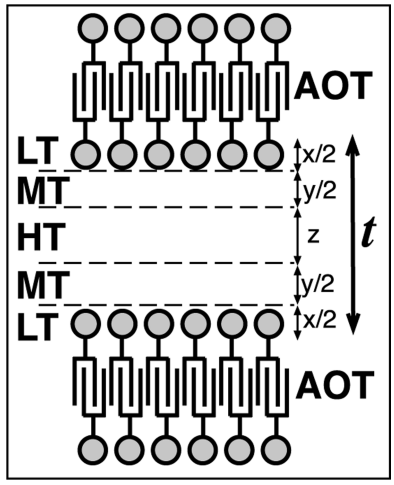

the lower temperature of melting observed. This population is the most affected by confinement and disturbance resulting from the narrowing of the water thickness, as it can be deduced from the decreasing of the melting temperature (Figure 3) with t.

Composition of the Water Populations. DSC allowed us to identify the actual populations in water (LT, MT, HT), identified by their different melting temperatures whereas FT-IR provides the amount of spectroscopic components (NW, IW, MW) identified by their local connectivity. These three spectroscopic components (NW, IW, MW) are distributed over the three populations of water (LT, MT, HT) with proportions related with the level of disturbance of the aqueous network.

From 0 to 15 wt % AOT, water is mostly formed by high temperature (HT) water (Figure 4). This population contains the three spectroscopic components in proportion that do not vary significantly (Figure 5 and Table SI.II, Supporting Information). Hence, we can evaluate directly the percentage of each spectroscopic component in the HT water:

High Temperature Population: 75% NW + 12.4% IW + 12.5% MW.

This result was used to calculate the spectroscopic composition of both LT and MT water in the 70% and 80% AOT samples where the HT contribution can be neglected. The thermal population of the 70 AOT% sample is (0.08 LT + 0.873 MT + 0.047 HT) and that of the 80 AOT% sample is (0.318 LT + 0.682 MT) (Table 1). Their IR components are (0.556 NW + 0.322 IW + 12.2 MW) and (0.548 NW + 0.326 IW + 0.126 MW), respectively. We could deduce the expected IR components for both compositions, as equal to:

Medium Temperature Population: 54.6% NW + 33.4% IW + 12% MW.

Low Temperature Population: 55.3% NW + 30.8% IW + 13.9% MW.

These values were validated for all samples by comparing the (NW, IW, MW) spectroscopic components extracted from the composition of the respective (LT, MT, HT) populations, with the spectroscopic values determined from IR measurement (Table SI.II, Supporting Information) (Figure 7).

The results are perfectly in line, and confirm that water trapped in the AOT lamellar phases is made of three different populations (HT, MT, and LT) identified by DSC, each population being described as a mixture of three types of water molecules of a given hydrogen bonding level. These clusters are clearly identified by FT-IR through the NW, IW, and MW spectroscopic components previously described.

The HT water population corresponds to bulk water. This population is composed of a majority (75%) of network water presenting a high degree of hydrogen bonds. This population presents a melting temperature of −2 °C, which remains constant over the full range of concentration. The MT population corresponds to an intermediate layer, which is more disturbed than bulk water: only 55% of network water and a higher amount of intermediate water than for the HT population, this disturbance leading to a lower enthalpy of melting (≈150 J g^{-1}), half that of pure water. On the basis of the evolution of the water population with the water thickness (see Scheme SI.1, Supporting Information) and the van der Waals diameter of the water molecule (2.82 Å), we can assume that this layer extends to around two layers of water.[24] Its thickness remains rather constant over the whole domain of concentration.

The LT population exhibits a similar distribution of spectroscopic components than MT, in agreement with their close melting temperatures: (−12 and −10 °C, respectively). Structural description of this type of water is more difficult because the molecules are in closer interaction within the surfactant layer, which cannot be described as an aqueous network. However, the local behavior and possibly a connection with the MT population, leads to a spectroscopic distribution close to MT, as confirmed by the melting temperatures that are only slightly different. It is worth mentioning that our initial assumption on the equivalent values of melting enthalpy that allowed us to merge the two populations could lead at the end to a similar distribution of spectroscopic components.

These results allow us to provide a more complete description of the structure of water confined between the lamellar phases of AOT, as made of bulk water (HT) sandwiched between the AOT layer with a thin (≈5 Å) intermediate layer of water with a disturbed structure. There is an additional population (LT) that corresponds to water in close interaction with the surfactant heads (≈2.6 per surfactant head) and connected to the intermediate layer.[9]

Conclusion

We have demonstrated that water trapped between lamellar AOT bilayers can be sorted in three populations defined by specific thermal behaviors: melting temperature and enthalpy of melting. Each population, named low temperature (LT), medium temperature (MT), or high temperature (HT) as a function of their temperature of melting, can be described by different distributions of spectroscopic components. These components were identified previously as network water (NW), intermediate water (IW), and multimer water (MW). They describe, from NW to MW, a decreasing degree of connections by hydrogen bonds between water molecules. We showed that HT water can be identified like "bulk" water and it presents the highest level of connectivity (75% of MW along with a high enthalpy and temperature of melting: 320 J g^{-1} and −4 °C, respectively). We have identified a second (MT) population that corresponds to a thin layer of water (around two molecular layers) in close contact with the AOT surface. This population corresponds to water actually disturbed by the confinement provided by the surfactant surface. Its enthalpy of melting was evaluated to be half that of bulk water (≈150 J g^{-1}) and its temperature of melting is lower (−10 °C) than for the HT water. Finally, a LT water is ascribed to hydration water closely linked to AOT heads. As expected for hydration water, the amount of LT water, which is proportional to the amount of surfactant,

TABLE 2: Distribution of the Different Thermal Populations Deduced from DSC Measurements: High (HT), Medium (MT), and Low (LT) Temperatures

AOT (wt %)	t (nm)	HT (%) $z = \Delta H(\mathrm{HT})/330$[a]	[LT+MT] (%) $Y = 1 - z$	MT (%) y[b]	LT (%) x[b]	$\Delta H°(\mathrm{MT}) = \Delta H(\mathrm{MT})/y$ (J g^{-1})	$t_i(\mathrm{HT}) = z't_i$ (nm)[c]	$t_i(\mathrm{MT}) = y't_i$ (nm)[c]
7.5		96	4	2.4	1.6	(41)		
10	18.6	98	2	1.1	0.9	145	18.4	0.20
15	13.25	97	3	2.3	0.7	182	12.95	0.30
25	7.77	91	9	6.7	2.3	168	7.24	0.53
30	5.56	85	15	12.7	2.3	155	4.84	0.72
40	3.45	72	28	25.6	2.4	125	2.55	0.90
50	2.4	56	44	41.0	3.0	154	1.39	1.01
54	2.06	52	48	45.0	3.0	150	1.01	1.05
60	1.5	39	61	54.0	7.0	157	0.63	0.87
70		2	98	90.0	8.0	145		
80		0	100	68.0	32.0	(10)		

[a] $\Delta H°(H_2O) = 330$ J g^{-1}. [b] We calculated the effective proportions of LT and MT water populations from the proportions of their DSC peaks. [c] Since the LT water was assumed being within the AOT bilayer, we calculated the water thickness assigned to HT and MT populations according to: $z'(\mathrm{HT}) = z/(z + y)$ and $y'(\mathrm{MT}) = y/(z + y)$.

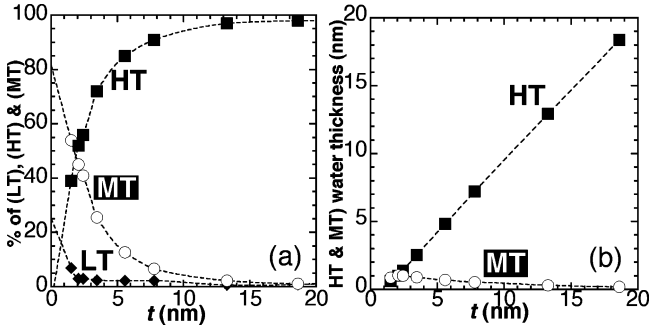

Figure 6. Evolution of the different populations of water as a function of the water thickness t (left axis) as well as the actual thickness of HT and MT components (right axis). Lines are plotted for visual help.

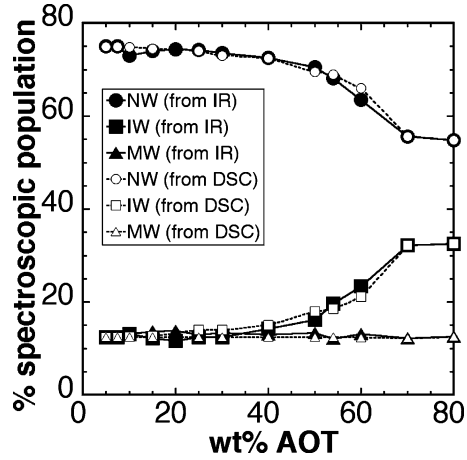

Figure 7. Comparison between the respective spectroscopic contributions (NW, IW, MW) deduced directly from FT-IR measurements (black dots) and those deduced from the DSC analysis (white dots). The good agreement between both results confirms the correct estimation of spectroscopic contributions to each thermal population (LT, MT, HT).

remains constant, whatever the water thickness. Finally, compared with our previous studies that were based only on IR analysis where the thickness of perturbed water was suggested as being around 2 nm, our present report shows that it is actually thinner, with a value of 0.5 nm. This apparent discrepancy can be easily explained because IR analyses reveal the sum of NW, IW, and MW spectroscopic components that belong all (in different proportions) to the three thermal populations (HT, MT, and LT). When the overall thickness decreases below 4 nm, the respective importance of HT ("bulk") water becomes less predominant and that of MT water more significant. It results overall that the distribution of the spectroscopic components is modified, even if the absolute amount of MT water itself remains unchanged. Discrimination is only allowed by the DSC analysis that provides a correct evaluation of the thermal populations. Still, there are two possible parameters (confinement and sodium ions) that can disturb the water structure and modify its thermochemical properties. Further studies will focus on the assignment of both of these parameters as actual sources in the disruption of the water network and how the differences in water melting can modify the structural changes of the AOT lamellar phases upon temperature variation.

Acknowledgment. We thank Ph. Dieudonné for help in SAXS measurements and S. Cerneaux for additional IR measurements of NaCl solutions.

Supporting Information Available: Examples of fits of the DSC peaks, evolution of the FT-IR peak positions and areas as a function of NaCl conc., SAXD patterns of the AOT phases, FT-IR analysis of the additional peaks (1640 and 1730 cm^{-1}), a schematic of the evolution of the lamellar phases with water thickness, and tables reporting the SAXD patterns and FT-IR spectra analysis, as well as the evolution of the IR populations. This material is available free of charge via the Internet at http://pubs.acs.org.

References and Notes

(1) Israelachvili, J. N.; Gourdon, D. *Science* **2001**, *292*, 867. Heuberger, M.; Zäch, M.; Spencer, N. D. *Science* **2001**, *29*, 905. Roy, R.; Tiller, W. A.; Bell, I.; Hoover, M. R. *Materials Research Innovations Online* **2005**, *9*−*4*, 577. Raschke, T. M. *Curr. Opin. Struct. Biology* **2006**, *16*, 152–159.

(2) Stanley, H. E.; Teixeira, J. *J. Chem. Phys.* **1980**, *73*, 3404. Blumberg, R. L.; Stanley, H. E.; Geiger, A.; Mausbach, P. *J. Chem. Phys.* **1984**, *80*, 5230. Giguère, P. A. *J. Chem. Phys.* **1987**, *87*, 4835. Ayotte, P.; Weddle, G. H.; Baley, C. G.; Johnson, M. A.; Vila, F.; Jordan, K. D. *J. Chem. Phys.* **1999**, *110*, 6268. Ayotte, P.; Weddle, G. H.; Johnson, M. A. *J. Chem. Phys.* **1999**, *110*, 7129. Devlin, J. P.; Joyce, C.; Buch, V. *J. Phys. Chem. A* **2000**, *104*, 1974. Chumaevskii, N. A.; Rodnikova, M. N. *J. Mol. Liq.* **2003**, *106*, 167. Zasetsky, A. Y.; Khalizov, A. F.; Sloan, J. J. *J. Chem. Phys.* **2004**, *121*, 6941. Soper, A. K. *J. Phys.: Condens. Matter* **2005**, *17*, S3273. Mantz, Y. A.; Chen, B.; Martyna, G. J. *Chem. Phys. Lett.* **2005**, *405*, 294. Sun, Q.; Zheng, H.-F. *Chin. Phys. Lett.* **2006**, *23*, 3022.

(3) Guillaume, B. C. R.; Yogey, D.; Fendler, J. H. *J. Chem. Soc., Faraday Trans.* **1992**, *88*, 1281.

(4) Novaki, L. P.; El Seoud, O. A. *J. Colloid Interface Sci.* **1998**, *202*, 391.

(5) Nishimoto, Y.; Kaneki, Y.; Kishi, A. *Anal. Sci.* **2004**, *20*, 1079.

(6) Calandra, P.; Caponetti, E.; Chillura Martino, D.; D'Angelo, P.; Minore, A.; Turco Liveri, V. *J. Mol. Struct.* **2000**, *522*, 165.

(7) Inoue, T.; Matsuda, M.; Nibu, Y.; Misono, Y.; Suzuki, M. *Langmuir* **2001**, *17*, 1833.

(8) Scatena, L. F.; Brown, M. G.; Richmond, G. L. *Science* **2001**, *292*, 908. Berger, C.; Desbat, B.; Kellay, H.; Turlet, J.-M.; Blaudez, D. *Langmuir* **2003**, *19*, 1. Nakamur, K.; Minagawa, Y.; Hatakeyama, T.; Hatakeyama, H. *Thermochim. Acta* **2004**, *416*, 135. Rousseau, R.; Kleinschmidt, V.; Schmitt, U. W.; Marx, D. *Angew. Chem., Int. Ed.* **2004**, *43*, 4804. Becraft, K. A.; Richmond, G. L. *J. Phys. Chem. B* **2005**, *109*, 5108. Soper, A. K.; Weckström, K. *Biophysical Chem.* **2006**, *124*, 180.

(9) Boissière, C.; Brubach, J.-B.; Mermet, A.; de Marzi, J. L.; Prouzet, E.; Roy, P. *J. Phys. Chem. B* **2002**, *106*, 1032.

(10) Ciesla, K.; Rahier, H.; Zakrzewska-Trznadel, G. *J. Therm. Anal. Calorim.* **2004**, *77*, 279.

(11) Kodama, M.; Abe, M.; Kawasaki, Y.; Hayashi, K.; Ohira, S.; Nozaki, H.; Katagiri, C.; Inoue, T.; Takahashi, H. *Thermochim. Acta* **2004**, *416*, 105.

(12) (a) MacDonald, H.; Bedwell, B.; Gulari, E. *Langmuir* **1986**, *2*, 704. Jain, T. K.; Varshney, M.; Maitra, A. *J. Phys. Chem.* **1989**, *93*, 7409.

(13) Onori, G.; Santucci, A. *J. Phys. Chem.* **1993**, *97*, 5430.

(14) Moran, P. D.; Bowmaker, G. A.; Cooney, R. P.; Bartlett, J. R.; Woolfrey, J. L. *Langmuir* **1995**, *11*, 738. Li, Q.; Weng, S.; Wu, J.; Zhou, N. *J. Phys. Chem. B* **1998**, *102*, 3168. Li, Q.; Li, T.; Wu, J. *J. Phys. Chem. B* **2000**, *104*, 9011. Zhou, N.; Li, Q.; Wu, J.; Chen, J.; Weng, S.; Xu, G. *Langmuir* **2001**, *17*, 4505. Zhou, G.-W.; Li, G.-Z.; Chen, W.-J. *Langmuir* **2002**, *18*, 4566. Nickolov, Z. S.; Paruchuri, V.; Shah, D. O.; Miller, J. D. *Colloids Surf. A* **2004**, *232*, 93. Sykora, J.; Jurkiewicz, P.; Epand, R. M.; Kraayenhof, R.; Langner, M.; Hofa, M. *Chem. Phys. Lipids* **2005**, *135*, 213–221. Crupi, V.; Majolino, D.; Venuti, V. *J. Phys.: Cond. Matter* **2004**, *16*, S5297. Crupi, V.; Majolino, D.; Migliardo, P.; Venuti, V.; Mizota, T. *Mol. Phys.* **2004**, *102*, 1943. Crupi, V.; Majolino, D.; Migliardo, P.; Venuti, V. *J. Mol. Liq.* **2005**, *117*, 165. Guo, Y.; Yui, H.; Minamikawa, H.; Masuda, M.; Kamiya, S.; Sawada, T.; Ito, K.; Shimizu, T. *Langmuir* **2005**, *21*, 4610. Johari, G. P. *J. Chem. Phys.* **2005**, *122*, web 194504.

(15) Temsamani, M. B.; Maeck, M.; El Hassani, I.; Hurwitz, H. D. *J. Phys. Chem. B* **1998**, *102*, 3335.

(16) Brubach, J.-B.; Mermet, A.; Filabozzi, A.; Colavita, P.; Gerschel, A.; Roy, P. *J. Phys. IV* **2000**, *10*, Pr7/215.

(17) Brubach, J.-B.; Mermet, A.; Filabozzi, A.; Colavita, P.; Gerschel, A.; Lairez, D.; Roy, P. *J. Phys. Chem. B* **2001**, *105*, 430.

(18) Yuan, S.-L.; Zhou, G.-W.; Xu, G.-Y.; Li, G.-Z. *J. Dispersion Sci. Technol.* **2004**, *25*, 733.

(19) Brubach, J.-B.; Mermet, A.; Filabozzi, A.; Gerschel, A.; Roy, P. *J. Chem. Phys.* **2005**, *122*, web 184509.

(20) Czarniecki, K.; Jaich, A.; Janik, J. M.; Rachwalska, M.; Janik, J. A.; Krawczyk, J.; Otnes, K.; Volino, F.; Ramasseul, R. *J. Colloid Interface Sci.* **1983**, *92*, 358.

(21) Casillas, N.; Puig, J. E.; Olayo, R.; Hart, T. J.; Franses, E. I. *Langmuir* **1989**, *5*, 384.

(22) *Handbook of Chemistry & Physics*, 78th ed.; CRC Press: Boca Raton, FL, 1997.

(23) Becker, E. D.; Pimentel, G. C.; Vanthiel, M. *J. Chem. Phys.* **1957**, *26*, 145. Vanthiel, M.; Becker, E. D.; Pimentel, G. C. *J. Chem. Phys.* **1957**, *27*, 95. Vanthiel, M.; Becker, E. D.; Pimentel, G. C. *J. Chem. Phys.* **1957**, *27*, 486. Kollman, P. A.; Allen, L. C. *J. Chem. Phys.* **1969**, *51*, 3286. Kollman, P. A.; Allen, L. C. *J. Chem. Phys.* **1970**, *52*, 5085.

(24) Finney, J. L. *J. Mol. Liq.* **2001**, *90*, 303.

JP101176V